

Circulation

JOURNAL OF THE AMERICAN HEART ASSOCIATION



Disrupted Junctional Membrane Complexes and Hyperactive Ryanodine Receptors After Acute Junctophilin Knockdown in Mice

Ralph J. van Oort, Alejandro Garbino, Wei Wang, Sayali S. Dixit, Andrew P. Landstrom, Namit Gaur, Angela C. De Almeida, Darlene G. Skapura, Yoram Rudy, Alan R. Burns, Michael J. Ackerman and Xander H.T. Wehrens

Circulation published online Feb 21, 2011;

DOI: 10.1161/CIRCULATIONAHA.110.006437

Circulation is published by the American Heart Association, 7272 Greenville Avenue, Dallas, TX 75214

Copyright © 2011 American Heart Association. All rights reserved. Print ISSN: 0009-7322. Online ISSN: 1524-4539

The online version of this article, along with updated information and services, is located on the World Wide Web at:

<http://circ.ahajournals.org>

Data Supplement (unedited) at:

<http://circ.ahajournals.org/cgi/content/full/CIRCULATIONAHA.110.006437/DC1>

Subscriptions: Information about subscribing to *Circulation* is online at
<http://circ.ahajournals.org/subscriptions/>

Permissions: Permissions & Rights Desk, Lippincott Williams & Wilkins, a division of Wolters Kluwer Health, 351 West Camden Street, Baltimore, MD 21202-2436. Phone: 410-528-4050. Fax: 410-528-8550. E-mail:
journalpermissions@lww.com

Reprints: Information about reprints can be found online at
<http://www.lww.com/reprints>

Disrupted Junctional Membrane Complexes and Hyperactive Ryanodine Receptors After Acute Junctophilin Knockdown in Mice

Ralph J. van Oort, PhD*; Alejandro Garbino, PhD*; Wei Wang, PhD*; Sayali S. Dixit, PhD; Andrew P. Landstrom, BS; Namit Gaur, MS; Angela C. De Almeida, MS; Darlene G. Skapura, BS; Yoram Rudy, PhD; Alan R. Burns, PhD; Michael J. Ackerman, MD, PhD; Xander H.T. Wehrens, MD, PhD

Background—Excitation-contraction coupling in striated muscle requires proper communication of plasmalemmal voltage-activated Ca^{2+} channels and Ca^{2+} release channels on sarcoplasmic reticulum within junctional membrane complexes. Although previous studies revealed a loss of junctional membrane complexes and embryonic lethality in germ-line junctophilin-2 (JPH2) knockout mice, it has remained unclear whether JPH2 plays an essential role in junctional membrane complex formation and the Ca^{2+} -induced Ca^{2+} release process in the heart. Our recent work demonstrated loss-of-function mutations in JPH2 in patients with hypertrophic cardiomyopathy.

Methods and Results—To elucidate the role of JPH2 in the heart, we developed a novel approach to conditionally reduce JPH2 protein levels using RNA interference. Cardiac-specific JPH2 knockdown resulted in impaired cardiac contractility, which caused heart failure and increased mortality. JPH2 deficiency resulted in loss of excitation-contraction coupling gain, precipitated by a reduction in the number of junctional membrane complexes and increased variability in the plasmalemma-sarcoplasmic reticulum distance.

Conclusions—Loss of JPH2 had profound effects on Ca^{2+} release channel inactivation, suggesting a novel functional role for JPH2 in regulating intracellular Ca^{2+} release channels in cardiac myocytes. Thus, our novel approach of cardiac-specific short hairpin RNA-mediated knockdown of junctophilin-2 has uncovered a critical role for junctophilin in intracellular Ca^{2+} release in the heart. (*Circulation*. 2011;123:979-988.)

Key Words: calcium ■ excitation ■ heart failure ■ junctophilin ■ sarcoplasmic reticulum

Excitation-contraction (EC) coupling is the fundamental mechanism by which depolarization of the voltage-gated Ca^{2+} channels (VGCCs) in the plasmalemma triggers a much greater release of Ca^{2+} from the sarcoplasmic reticulum (SR) via type 2 ryanodine receptors (RyR2), a process known as Ca^{2+} -induced Ca^{2+} release (CICR).¹ This Ca^{2+} release amplification depends on the organization of VGCC and RyR2 within junctional membrane complexes (JMCs), also known as calcium release units.² Disruption of JMC structure, as seen in heart failure, profoundly affects CICR and thus cardiac muscle contractility.³

Clinical Perspective on p 988

The molecular mechanisms involved in organizing Ca^{2+} channels within the JMC remain poorly understood. One

family of proteins, known as junctophilins (JPHs), has been proposed to provide a structural bridge between the plasmalemma and SR, thereby potentially ensuring approximation of VGCC and RyR2.⁴ Junctophilin-2 (JPH2) is the major cardiac isoform among the 4 JPH isoforms, which are expressed within JMCs of all excitable cell types.⁵ JPH proteins comprise 8 N-terminal “membrane occupation and recognition nexus” domains, a space-spanning α -helix, and a C-terminal transmembrane domain. The membrane occupation and recognition nexus domains mediate binding to the plasmalemma, and the hydrophobic transmembrane domain is anchored into the SR membrane.⁶

The role of junctophilin in myocytes has remained unclear because of the lack of adequate animal models. Mice deficient in *JPH1*, the major skeletal muscle isoform, suffer from

Received November 4, 2010; accepted January 7, 2011.

From the Department of Molecular Physiology and Biophysics, Baylor College of Medicine, Houston, TX (R.J.v.O., A.G., W.W., S.S.D., A.C.D.A., D.G.S., X.H.T.W.); Departments of Molecular Pharmacology and Experimental Therapeutics, Medicine, and Pediatrics, Mayo Clinic, Rochester, MN (A.P.L., M.J.A.); Cardiac Bioelectricity and Arrhythmia Center, Washington University, St Louis, MO (N.G., Y.R.); College of Optometry, University of Houston, Houston, TX (A.R.B.); and Department of Medicine, Division of Cardiology, Baylor College of Medicine, Houston, TX (X.H.T.W.).

*Drs van Oort, Garbino, and Wang contributed equally to this work.

The online-only Data Supplement is available with this article at <http://circ.ahajournals.org/cgi/content/full/CIRCULATIONAHA.110.006437/DC1>. Correspondence to Xander H.T. Wehrens, MD, PhD, Department of Molecular Physiology and Biophysics, Baylor College of Medicine, One Baylor Plaza, BCM335, Houston, TX 77030. E-mail wehrens@bcm.edu

© 2011 American Heart Association, Inc.

Circulation is available at <http://circ.ahajournals.org>

DOI: 10.1161/CIRCULATIONAHA.110.006437

muscle abnormalities and perinatal death.⁷ Genetic ablation of *JPH2* results in embryonic lethality, most likely because of absence of cardiac contractility around embryonic day 10.5.⁴ Therefore, the physiological role of JPH2 in the adult heart remains to be elucidated. In recent studies, we and another group have identified missense mutations in *JPH2* in patients with hypertrophic cardiomyopathy.^{8,9} Moreover, decreased JPH2 expression was observed in a rat model of aortic stenosis and mouse models of hypertrophic and dilated cardiomyopathy.^{10,11} However, it remains to be determined whether downregulation of JPH2 is a mere response to heart failure or actually precipitates disease progression. Again, unraveling these questions has thus far been greatly hampered by the lack of a suitable animal model.

To circumvent the embryonic lethality associated with conventional genetic deletion of *JPH2*, we generated a novel transgenic mouse model that allows inducible cardiac-specific knockdown of JPH2 using RNA interference. We demonstrated that JPH2 deficiency is associated with the development of acute heart failure due to a loss of JMCs and reduced CICR. The CICR process was impaired because of reduced colocalization and functional coupling of VGCC and RyR2, without affecting expression levels. Moreover, loss of JPH2 impaired proper RyR2 inactivation, suggesting previously unrecognized roles for JPH2 in cardiac muscle and directly linking JPH2 deficiency to contractile dysfunction in failing hearts.

Methods

Please refer to the online-only Data Supplement for a more detailed Methods section.

Generation of Transgenic Mice

The generation of mice with cardiac-specific inducible short hairpin RNA (shRNA)-mediated knockdown of JPH2 is described in detail in the online-only Data Supplement.

Northern Blot and Real-Time Polymerase Chain Reaction

Detailed methods are provided in the expanded Methods section in the online-only Data Supplement.

Western Blotting and Coimmunoprecipitation

Western blotting and coimmunoprecipitation were performed as described in detail previously.¹²

Immunohistochemistry and Histology

Detailed methods are provided in the online-only Data Supplement.

Transthoracic Echocardiography

Mice were anesthetized with the use of 1% to 2.0% isoflurane in 95% O₂. Cardiac function was assessed with M-mode echocardiograms acquired with a VisualSonics VeVo 770 Imaging System (VisualSonics, Toronto, Ontario, Canada), as described.¹³

Electrophysiology and Ca²⁺ Imaging

Detailed methods are provided in the online-only Data Supplement.

Electron Microscopy

Detailed methods are provided in the online-only Data Supplement.

Computational Model

Detailed methods are provided in the online-only Data Supplement.

Statistical Analysis

Data are expressed as mean ± SEM. Statistical significance of differences between experimental groups was compared with Student *t* test and 1-way ANOVA with pairwise multiple comparisons performed with the Student-Newman-Keuls method as appropriate. If data were not normal according to the Shapiro-Wilk test, the Wilcoxon rank sum or Kruskal-Wallis test was used, as appropriate. A value of *P* < 0.05 was considered statistically significant.

Results

Cardiac-Specific, Inducible JPH2 Knockdown With RNA Interference

To circumvent embryonic lethality associated with germ-line JPH2 knockout, we developed a novel approach for inducible cardiac-specific JPH2 knockdown. We first cloned 4 candidate shRNA oligonucleotides targeting different regions in mouse *JPH2* and tested the knockdown efficiency in vitro (Figure 1a in the online-only Data Supplement). Western blot analysis demonstrated efficient knockdown for 3 JPH2-shRNA constructs (Figure 1b in the online-only Data Supplement). The most efficient oligonucleotide (No. 2) was used to generate a conditional JPH2 knockdown (shJPH2) mouse. shJPH2 mice harbor a transgene composed of the JPH2 shRNA sequence downstream of a U6 promoter, which is inactive because of the insertion of a loxP flanked *neo* cassette.¹⁴ To ensure cardiac-specific shRNA expression, we crossed shJPH2 mice with α -myosin heavy chain (α MHC)-MerCreMer (MCM) mice, which express a tamoxifen-inducible mutant Cre recombinase under control of the cardiac-specific α MHC promoter.¹⁵ Tamoxifen administration in double transgenic MCM-shJPH2 mice results in cardiac-specific excision of the *neo* cassette, which activates the U6 promoter and induces expression of JPH2 shRNA (Figure 1A).

Northern blot analysis confirmed expression of JPH2 shRNA exclusively in the hearts of tamoxifen-injected MCM-shJPH2 mice. Moreover, indicative of the cardiac specificity, there was no JPH2 shRNA expression in skeletal muscle of tamoxifen-injected MCM-shJPH2 mice (Figure 1B). Real-time polymerase chain reaction analysis revealed that *JPH2* mRNA levels were significantly lower in hearts of tamoxifen-treated MCM-shJPH2 mice, whereas *JPH1* mRNA levels were unaltered (Figure 1C). Western blot analysis of cardiac protein lysates demonstrated that knockdown of JPH2 mRNA resulted in a 60% reduction in JPH2 protein (Figure 1B). Because expression of double-stranded RNA might trigger a cellular interferon response with the potential to affect gene expression,¹⁶ we measured mRNA levels of oligoadenylate synthase-1 (*OAS1*) and signal transducer and activator of transcription 1 (*STAT1*). Real-time polymerase chain reaction analysis demonstrated unaltered levels of *OAS1* and *STAT1* in tamoxifen-treated MCM-shJPH2 mice (Figure 1c in the online-only Data Supplement). Whereas all provided data were obtained in mice from 1 transgenic line (line 38), we confirmed similar findings in a second independent shJPH2 transgenic mouse line (line 21) in which JPH2 was reduced by 30% after tamoxifen administration (data not shown). These data show that we successfully created a novel shRNA-mediated approach to selectively reduce JPH2 protein levels in the adult murine heart.

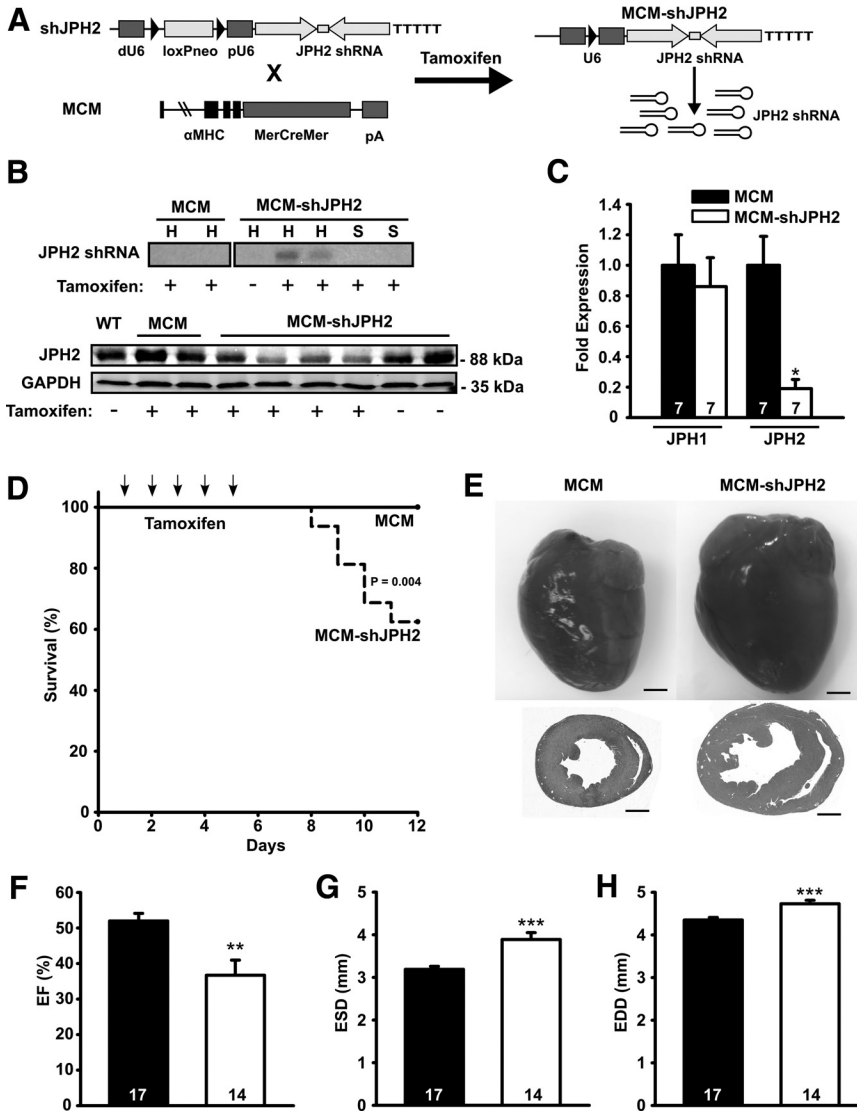


Figure 1. Inducible cardiac-specific junctophilin-2 (JPH2) knockdown causes mortality and acute heart failure. **A**, Schematic representation of targeting vector to overexpress JPH2-targeting shRNA sequence (shJPH2) downstream of a U6 promoter, inactivated by insertion of a loxP-flanked neomycin (*neo*) cassette dividing the distal (dU6) and proximal (pU6) parts of the promoter. Tamoxifen administration to double transgenic offspring of α -myosin heavy chain (α MHC)-MerCreMer(MCM) and shJPH2 (junctophilin-2 knockdown) mice leads to cardiac-specific Cre-mediated excision of the *neo* cassette, resulting in expression of JPH2 shRNA. **B**, Northern blot analysis (top) of JPH2 shRNA in hearts (H) and skeletal muscle (S) and Western blot analysis (bottom) for JPH2 protein levels in heart lysates from tamoxifen-treated MCM-shJPH2 mice. WT indicates wild type. **C**, Quantitative polymerase chain reaction analysis of JPH1 and JPH2 mRNA levels in cardiac tissue from MCM and MCM-shJPH2 mice. **D**, Kaplan-Meier curve revealing increased mortality in MCM-shJPH2 compared with MCM mice. Arrows indicate single tamoxifen injections at days 1 to 5. **E**, Representative whole mounts (top) and hematoxylin-eosin-stained transverse sections (bottom) of MCM and MCM-shJPH2 mouse hearts 1 week after completion of tamoxifen administration. Bar=1 mm. **F** through **H**, Echocardiographic measurement of ejection fraction (EF) (**F**), end-systolic diameter (ESD) (**G**), and end-diastolic diameter (EDD) (**H**) 1 week after tamoxifen. Data are represented as mean \pm SEM; * P <0.05, ** P <0.01, *** P <0.001 vs MCM control. Number of mice is indicated inside bars.

Downregulation of JPH2 Leads to Acute Heart Failure

JPH2 knockdown in MCM-shJPH2 mice caused a significantly reduced survival rate compared with MCM mice (Figure 1D). Within 1 week after tamoxifen injections, mortality was 40% among MCM-shJPH2 mice compared with 0% among MCM mice ($P=0.004$). Histological analysis of surviving mice revealed cardiac dilatation in MCM-shJPH2 mice (Figure 1E). Transthoracic echocardiography revealed significantly decreased ejection fractions in MCM-shJPH2 mice ($36.72 \pm 4.25\%$) compared with MCM controls ($51.97 \pm 2.15\%$; $P<0.01$) (Figure 1F; Table in the online-only Data Supplement). Furthermore, end-systolic diameter and end-diastolic diameter were both significantly larger in MCM-shJPH2 (3.89 ± 0.16 and 4.80 ± 0.07 mm, respectively) compared with MCM control mice (3.19 ± 0.07 and 4.35 ± 0.06 mm; $P<0.001$) (Figure 1G and 1H). Similar findings were obtained in MCM-shJPH2 mice from line 21 (Table in the online-only Data Supplement). Left ventricular posterior wall thickness did not change between MCM-shJPH2 (0.80 ± 0.03 mm) and MCM controls (0.79 ± 0.02 mm; $P=NS$; Figure 1d in the online-only Data

Supplement), suggesting that the observed changes were not due to compensatory cardiac remodeling. Consistently, there was no difference in cardiomyocyte cross-sectional areas between MCM-shJPH2 mice and MCM controls (Figure 1e in the online-only Data Supplement). On the other hand, the ratio of lung weight to tibia length was increased in MCM-shJPH2 mice, consistent with pulmonary congestion in MCM-shJPH2 mice (Figure 1f in the online-only Data Supplement). However, mRNA levels of cardiac stress markers skeletal muscle α -1 actin (*Acta1*), atrial natriuretic factor (*ANF*), brain natriuretic peptide (*BNP*), β -myosin heavy chain (*[beta]MHC*), and the exon 4 splice isoform of regulator of calcineurin 1 (*RCAN1-4*) were not altered after JPH2 knockdown (Figure 1g in the online-only Data Supplement). Thus, acute loss of JPH2 in the heart results in sudden cardiac death caused by acute heart failure in the absence of hypertrophic remodeling.

Loss of EC Coupling Gain in JPH2 Knockdown Mice

We next determined the effects of JPH2 knockdown on EC coupling by simultaneously measuring VGCC Ca^{2+} influx and

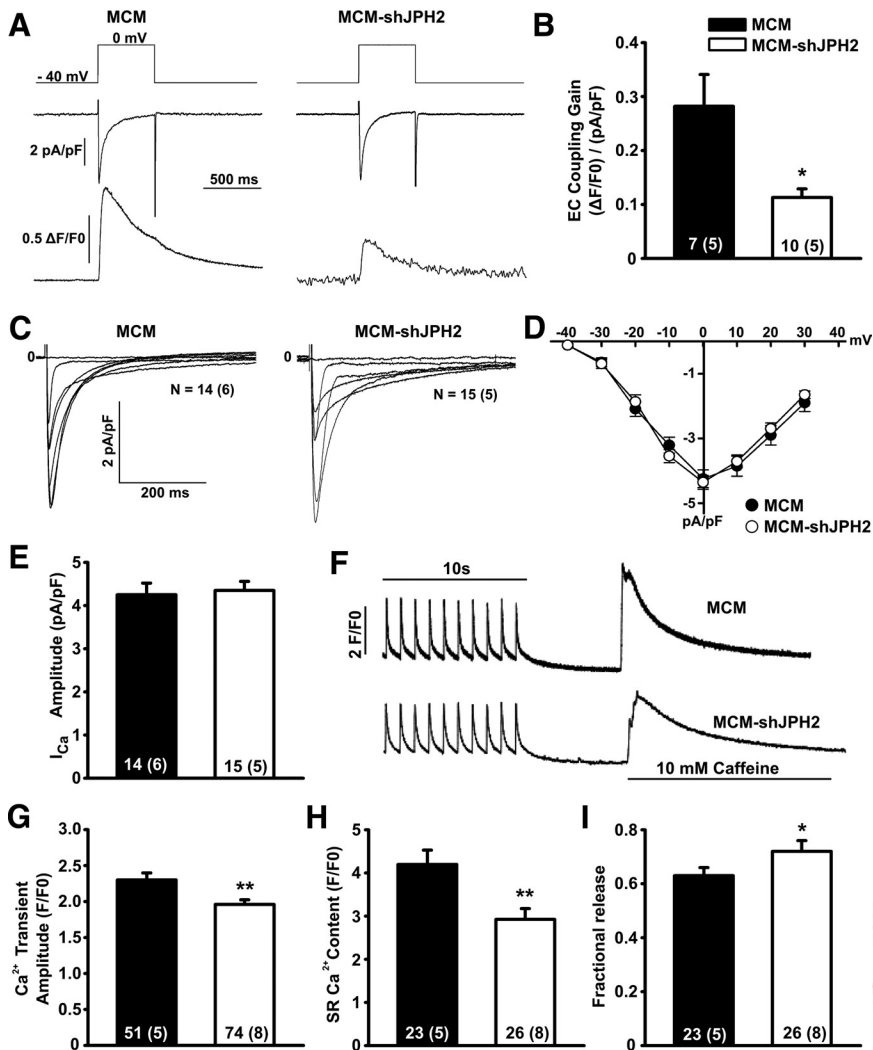


Figure 2. Junctophilin-2 (JPH2) knock-down reduces excitation-contraction (EC) coupling by suppression of Ca^{2+} -induced Ca^{2+} release (CICR). A, Representative simultaneous tracings evoked by a 40-mV depolarization step (top) of Ca^{2+} current through the voltage-gated Ca^{2+} channels (VGCC) (middle) and whole-cell Ca^{2+} transient (bottom). B, Bar graph of EC coupling gain. C, Representative whole-cell patch clamp current tracings of amplitude and inactivation kinetics of VGCC. D, Current-voltage curves showing activation kinetics of VGCC. E, Bar graph showing peak amplitude of Ca^{2+} current through VGCC at 0 mV. F, Representative tracings of Ca^{2+} transient amplitudes when paced at 1 Hz and total SR Ca^{2+} content as measured by the amplitude of caffeine-induced Ca^{2+} transient. G, Bar graph demonstrating decreased average Ca^{2+} transients in MCM-shJPH2 mice. H, Bar graph showing decreased average SR Ca^{2+} load in MCM-shJPH2 (α -MerCreMer-junctophilin-2 knock-down) mice. I, Fractional release (SR Ca^{2+} transient normalized for sarcoplasmic reticulum (SR) Ca^{2+} load) was increased in MCM-shJPH2 mice. Data are represented as mean \pm SEM; numbers indicate total number of cells, with number of mice in parentheses. * $P < 0.05$, ** $P < 0.01$ vs MCM control.

RyR2 Ca^{2+} release. Whereas Ca^{2+} influx through VGCC was unaffected by loss of JPH2, Ca^{2+} release from the SR (ie, Ca^{2+} transients) was significantly smaller in tamoxifen-treated MCM-shJPH2 mice (Figure 2A). As a result, the gain of EC coupling was reduced by $>50\%$ after JPH2 knockdown (MCM-shJPH2: 0.11 ± 0.02 versus MCM: 0.29 ± 0.06 ; $P < 0.05$; Figure 2B). Further analysis revealed that neither inactivation kinetics (MCM: 35.79 ± 2.53 ms versus MCM-shJPH2: 31.37 ± 2.18 ms; $P = 0.19$) nor current-voltage relationship of VGCC was affected by loss of JPH2 (Figure 2C and 2D). The total amount of Ca^{2+} entering the cell via VGCC was also comparable between MCM-shJPH2 (4.35 ± 0.21 pA/pF) and MCM mice (4.25 ± 0.27 pA/pF; $P = NS$; Figure 2E).

In addition to the Ca^{2+} influx trigger, the amount of SR Ca^{2+} release also depends on SR Ca^{2+} load and activity of RyR2 channels. Therefore, we assessed the amount of Ca^{2+} stored in the SR after steady state pacing at 1 Hz (Figure 2F). Consistent with EC coupling experiments (Figure 2A), the amplitude of pacing-evoked Ca^{2+} transients was decreased in MCM-shJPH2 mice (1.91 ± 0.06 F/F₀) compared with MCM controls (2.30 ± 0.10 ; $P < 0.01$; Figure 2G). SR Ca^{2+} content, measured by a caffeine dump protocol, was significantly decreased in MCM-shJPH2 mice (2.92 ± 0.25 F/F₀ versus

4.10 ± 0.33 F/F₀; $P < 0.01$; Figure 2H). Surprisingly, however, we observed that the relative amount of SR Ca^{2+} released via RyR2 normalized to SR Ca^{2+} content (ie, fractional release) was increased when JPH2 was downregulated (Figure 2I). Because the Ca^{2+} decay curves in the presence of caffeine appeared shallower in MCM-shJPH2 mice compared with MCM controls, we further analyzed Na^+ - Ca^{2+} exchange activity. We found that τ values were significantly decreased after JPH2 knockdown ($\tau = 2.70 \pm 0.23$ for MCM versus 5.11 ± 0.61 for MCM-shJPH2 mice, respectively; $P < 0.01$). Combined, these data suggest that 1 consequence of JPH2 deficiency is reduced VGCC-RyR2 coupling leading to reduced cardiomyocyte contractility due to a novel role of JPH2 in directly regulating RyR2 activity.

JPH2 Knockdown Disrupts JMC Organization

To ascertain the effects of JPH2 deficiency on the structure of JMCs, we first examined colocalization of VGCC and RyR2 in ventricular myocytes from MCM-shJPH2 mice. Immunofluorescent imaging indicated that both types of Ca^{2+} channels were distributed in similar striated patterns (Figure 3A through 3D). However, colocalization between the 2 channels was significantly decreased after JPH2 knockdown, and this

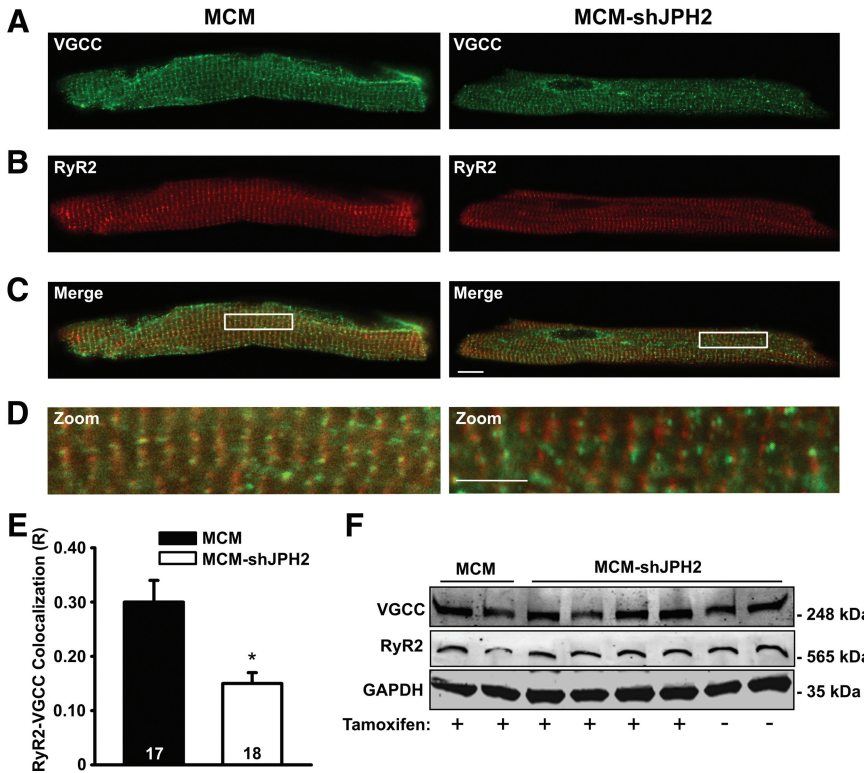


Figure 3. Impaired colocalization of voltage-gated Ca²⁺ channels (VGCC) and type 2 ryanodine receptors (RyR2) in cardiomyocytes after junctophilin-2 (JPH2) knockdown. A through C, Representative examples of immunofluorescent labeling of ventricular myocytes isolated from tamoxifen-treated MCM (α -MerCreMer) or MCM-shJPH2 (α -MerCreMer-junctophilin-2 knockdown) mice for VGCC (A), RyR2 (B), and both channels (C). Bar=10 μ m. D, Close-ups from images given in C demonstrate decreased overlap between VGCC and RyR2 channels in MCM-shJPH2 myocytes. Bar=5 μ m. E, Bar graph showing quantification of VGCC-RyR2 colocalization (R), which was significantly reduced after JPH2 knockdown. F, Western blots showing unaltered expression of VGCC and RyR2 after JPH2 knockdown in MCM-shJPH2 mice. Averaged data are represented as mean \pm SEM; numbers indicate total number of cells. * P <0.05 vs MCM control.

was not due to a difference in protein levels (Figure 3E and 3F). Thus, loss of JPH2 results in defective colocalization of VGCC and RyR2 Ca²⁺ channels within the JMC.

We therefore examined the structure of transverse (T)-tubules using di-8-ANEPPS staining. A significant disruption of normal T-tubular structure was apparent in cardiomyocytes from tamoxifen-treated MCM-shJPH2 mice (Figure 4A and Figure II in the online-only Data Supplement). These alterations in T-tubular structure did not affect membrane capacitance (average membrane capacitance=184.6 \pm 22.6 pF for MCM versus 165.8 \pm 22.6 pF for MCM-shJPH2 mice, respectively; P =0.27). Transmission electron microscopy was used to investigate ultrastructural changes in the JMCs (Figure 4B). Cardiomyocytes from MCM-shJPH2 mice had 40% fewer JMCs (0.36 \pm 0.04 JMCs per sarcomere) than MCM control mice (0.59 \pm 0.01; Figure 4C). Furthermore, the remaining JMCs were irregular in terms of their structure. Whereas the average distance between the T-tubular membrane and SR membrane was similar (12.45 \pm 0.52 nm in MCM-shJPH2 versus 12.30 \pm 0.26 nm in MCM), the gap between the 2 membranes within a single JMC (intradyad width) was more variable in MCM-shJPH2 mice (variance 1.96 nm²) than in MCM controls (variance 1.21 nm²; P <0.01; Figure 4D). In addition, dyad width among different JMCs (interdyad width) was significantly more variable in MCM-shJPH2 cardiomyocytes (variance 0.26 nm²) compared with MCM controls (variance 1.07 nm²; Figure 4E). Therefore, acute loss of JPH2 leads to altered morphology and loss of JMCs.

JPH2 Stabilizes the Ryanodine Receptor Ca²⁺ Release Channel

The reduction in JMC number and disruption of VGCC/RyR2 colocalization could account for the attenuated EC coupling

gain (Figure 2). However, structural uncoupling of VGCC and RyR2 would theoretically cause reduced RyR2 triggering, leading to increased SR Ca²⁺. Because we observed the exact opposite, a reduction in SR Ca²⁺ content (Figure 2F and 2H), we decided to assess RyR2 channel behavior during cellular diastole in cardiomyocytes from MCM-shJPH2 mice (Figure 5A and 5B). Ventricular myocytes of MCM-shJPH2 mice exhibited an increase in cell-wide spontaneous Ca²⁺ release events after a 1-Hz pacing train compared with MCM mice (Figure 5A and 5C). Next, we used confocal line scan imaging to visualize Ca²⁺ sparks in isolated cardiomyocytes (Figure 5B). Knockdown of JPH2 in MCM-shJPH2 mice led to a significantly higher Ca²⁺ spark frequency (Figure 5B and 5D). Taken together, our data indicate that loss of JPH2 leads to increased diastolic Ca²⁺ leak via RyR2 channels. Moreover, this suggests that JPH2 is an important RyR2 regulator besides its structural role in the JMC. Immunoprecipitation of RyR2 from mouse heart tissue revealed that JPH2 binds to RyR2, further supporting a novel role of JPH2 in directly regulating RyR2 (Figure 5F). Thus, our data suggest that JPH2 is required for proper inactivation of RyR2 and that loss of JPH2 can cause diastolic Ca²⁺ leaks.

Effect of JMC Alterations on EC Coupling Gain in a Computational Model

Our experimental data in MCM-shJPH2 mice revealed that acute loss of JPH2 leads to a reduced number of JMCs and an increased variability in the distance between the plasmalemmal and SR membranes. In our in vivo model, however, it is not possible to distinguish the individual contributions of these alterations to EC coupling gain, which was severely impaired after JPH2 knockdown. Therefore, we used a mathematical model to quantitatively probe the effects of

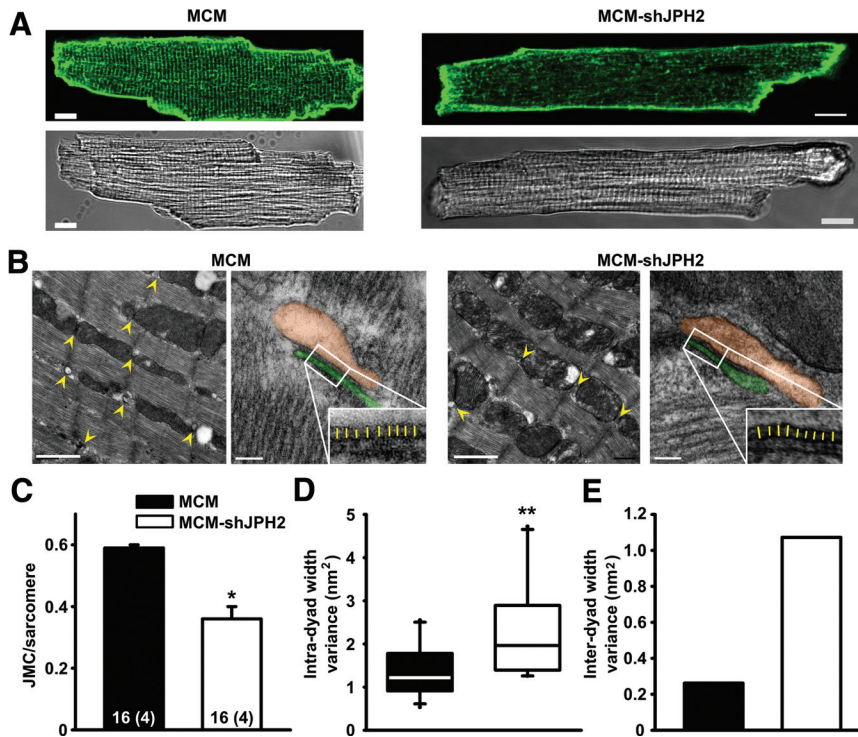


Figure 4. Junctophilin-2 (JPH2) knockdown causes fewer but more variable junctional membrane complexes (JMC). **A**, Isolated ventricular myocytes stained with di-8-ANEPPS to visualize T-tubule organization and shown in bright field. Bar=10 μ m. **B**, Low-magnification electron micrographs of JMC (yellow arrowheads) in myocytes from MCM-shJPH2 (α -MerCreMer-junctophilin-2 knockdown) and MCM control mice. Bar=1 μ m. High-magnification micrographs demonstrate altered morphology of remaining JMC after JPH2 knockdown (orange pseudocolor indicates sarcoplasmic reticulum [SR], and the T-tubule is colored in green). The insets demonstrate more variable distance between SR and T-tubule membranes in MCM-shJPH2 cardiomyocytes (yellow lines). Bar=100 nm. **C**, Quantification of the number of JMC per sarcomere. **D**, Bar graph showing that the average dyad width variance per JMC was larger in myocytes from MCM-shJPH2 mice. **E**, Bar graph showing overall variance among all measurements of average JMC distance in MCM-shJPH2 vs MCM controls. Averaged data are represented as mean \pm SEM; numbers indicate total number of cells, with number of mice in parentheses. * P <0.05, ** P <0.01 vs MCM control.

mentioned changes in JMC structure within the cardiac myocyte on EC coupling gain (Figure 6A). The Luo-Rudy myocyte simulation model was used, with a modified Ca^{2+} cycling process represented by up to 10 000 discrete Ca^{2+} release units.¹⁷

With the use of the exact values for JMC number and interdyad and intradyad width variance obtained in the tamoxifen-treated MCM and MCM-shJPH2 mice, the model predicts a 64% drop in EC coupling gain, which is very similar to our in vivo measurements ($60.0\pm 5.7\%$; Figure 6B). First, we simulated the effect of reducing the number of JMCs (or dyads) (Figure 6C). Our data reveal that a reduction in the number of dyads leads to a reduction in EC coupling gain according to a nearly linear relationship. Subsequently, the effects of changing interdyad or intradyad width variability were also simulated. In both cases, experimentally observed changes in interdyad or intradyad width variability (marked in the Figure) were predicted to decrease EC coupling gain (Figure 6D and 6E). Finally, we compared the relative contribution of each of these changes in the JMC to the loss of EC coupling gain (Figure 6F). The reduction in dyad number was the main contributor, followed by the increase in intradyad variability and interdyad variability. Combined, these changes account for the severe loss of EC coupling gain, consistent with decreased cardiac contractility observed after JPH2 knockdown.

Rescue of JPH2 Knockdown Phenotype by Overexpression of JPH2

Although shRNA-mediated knockdown of JPH2 expression represents a powerful tool to study the role of JPH2 in the heart, it is theoretically possible that the observed phenotype was due to nonspecific side effects of transgene integration or off-target effects of shRNA. Although this seemed less likely

without an interferon response and normal mRNA levels of the lesser cardiac JPH isoform (*JPH1*), we performed a series of rescue experiments to further prove the specificity of shRNA-mediated JPH2 knockdown effects. We intercrossed the MCM-shJPH2 mice with transgenic mice overexpressing JPH2 in the heart (OE). Western blot analysis of cardiac lysates revealed supranormal JPH2 levels in tamoxifen-treated MCM-shJPH2-OE triple transgenic mice (Figure 7A). Echocardiographic analysis revealed that fractional shortening and cardiac dimensions were similar in MCM-shJPH2-OE and MCM mice, suggesting that JPH2 overexpression in hearts of JPH2 knockdown mice rescued cardiac dysfunction (Figure 7B and Table in the online-only Data Supplement). Furthermore, electron microscopy analysis showed complete rescue of ultrastructural abnormalities, as did confocal imaging of Ca^{2+} transient amplitudes (Figure 7C and 7D). Thus, the cardiac phenotype in MCM-shJPH2 mice is specifically caused by shRNA-mediated knockdown of JPH2 in the heart.

Discussion

Proper conversion of plasmalemmal depolarization into release of intracellular Ca^{2+} from the SR is a prerequisite for myocyte contractility.¹⁸ This fundamental process known as CICR takes place within specialized subcellular domains known as JMCs. JMCs are found in all excitable cell types and are believed to be necessary to provide a structural and functional coupling between the plasma membrane and intracellular Ca^{2+} storage organelles such as the SR. In heart failure, the reduced CICR and disorganization of JMC are believed to contribute to contractile dysfunction, although the molecular mechanisms remain poorly understood.

After the initial discovery of the JPH family, it was postulated that this class of proteins provides a structural

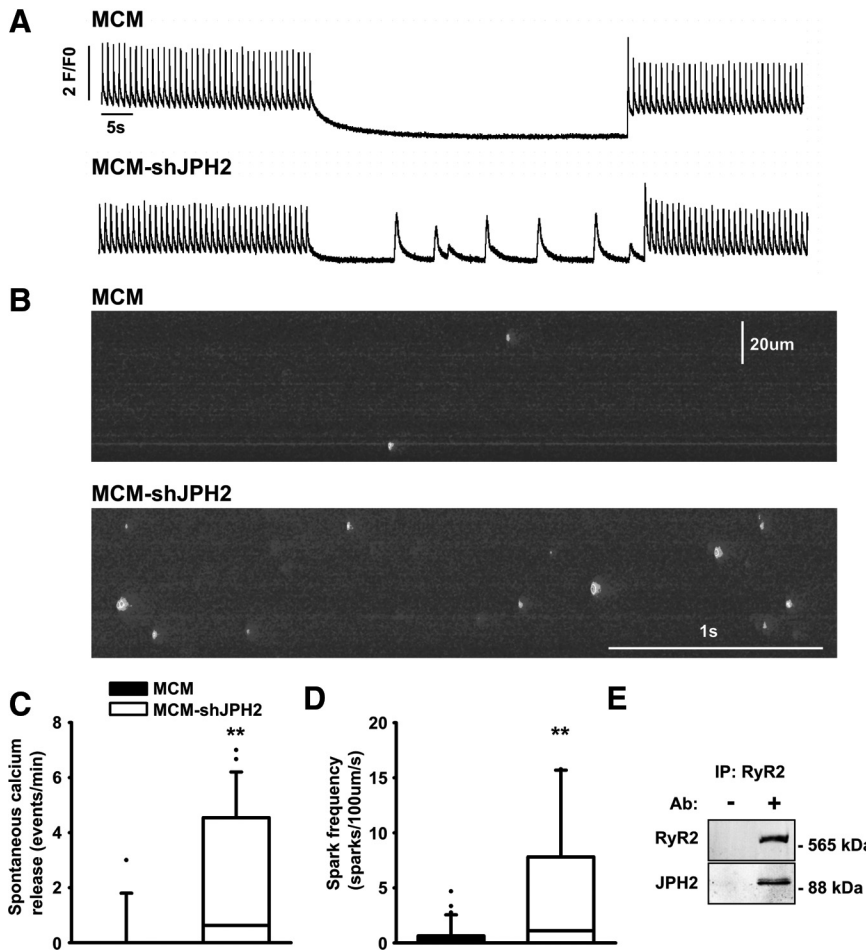


Figure 5. Junctophilin-2 (JPH2) knock-down causes defective type 2 ryanodine receptors (RyR2) gating, resulting in spontaneous sarcoplasmic reticulum (SR) Ca²⁺ release. **A**, Representative Ca²⁺ transient recordings demonstrating increased incidence of spontaneous SR Ca²⁺ release events in ventricular myocytes from MCM-shJPH2 (α -MerCreMer-junctophilin-2 knock-down) mice. **B**, Confocal microscopy line scans revealing increased number of Ca²⁺ sparks in MCM-shJPH2 mice. **C** and **D**, Box plots showing quantification of the number of spontaneous Ca²⁺ release events (**C**; n=26 cells from 4 mice MCM and 13 cells from 5 mice MCM-shJPH2) and Ca²⁺ sparks (**D**; n=37 cells from 4 mice MCM and 28 cells from 5 mice MCM-shJPH2). **E**, Coimmunoprecipitation of heart lysates from a wild-type mouse in the presence or absence of anti-RyR2 (type 2 ryanodine receptors) antibody (Ab). Western blots showing that immunoprecipitation (IP) with the use of anti-RyR2 antibody pulled down JPH2. ***P*<0.01 vs MCM control.

bridge that anchors the SR membrane to the plasmalemma within JMCs. Previous studies in germ-line JPH2 knockout mice revealed embryonic lethality at E10.5 due to weakened contractility and heart failure.⁴ Although embryonic JPH2-deficient mice exhibited defective calcium release units, whether this was directly caused by the absence of JPH2 has remained controversial because other knockout mouse models, including triadin-deficient mice, display similar subcellular defects.¹⁹ To overcome these limitations, we developed a novel shRNA-based interference approach to induce acute knockdown of JPH2 expression levels exclusively in adult mice cardiac myocytes (MCM-shJPH2 mice). Our findings revealed reproducible JPH2 knockdown after tamoxifen administration in 2 independent transgenic MCM-shJPH2 lines. It is important to highlight that conventional tissue-specific gene knockout only produces heterozygous (50% knockout) and homozygous (100% knockout) genotypes. In contrast, our shRNA-based model allowed us to study a wide range of knockdown percentages in MCM-shJPH2 mice. Thus, our new approach to inducible and cardiac-specific gene knockdown enabled us to determine the specific role of JPH2 in the maintenance of cardiac structure and function. Specificity of the model was confirmed by demonstrating that transgenic overexpression of JPH2 in MCM-shJPH2 knockdown mice prevented loss of JPH2 and negated the development of cardiac and cellular phenotypes linked to JPH2 deficiency.

Our findings suggest that loss of JPH2 is directly responsible for impaired cardiac contractility, one of the hallmarks of congestive heart failure. Loss of JPH2 expression in MCM-shJPH2 mice caused development of acute contractile failure in the absence of myocardial remodeling or alterations in expression levels of other Ca²⁺ handling proteins, suggesting that JPH2 deficiency impaired EC coupling within the JMC. Furthermore, our data indicate that loss of cardiac JPH2, as observed in animal models for heart failure,^{10,11} is not a compensatory response during heart disease development but actually plays a causal role in the disease progression. The finding that genetic mutations in *JPH2* cause hypertrophic cardiomyopathy and heart failure also implies a causal link between JPH2 defects and heart disease.^{8,9}

Previous studies in animals with congestive heart failure revealed reduced EC coupling due to an inability of VGCC to trigger sufficient SR Ca²⁺ release.²⁰ Our findings in cardiomyocytes isolated from MCM-shJPH2 mice suggest that loss of JPH2 expression is directly responsible for defective CICR. Furthermore, JPH2 knockdown in adult cardiomyocytes increased variability in the distance between the SR and plasma membrane within a single JMC and among populations of JMCs. These data suggest that the remaining JPH2 proteins are sufficient to keep both membranes together as JMCs but that the fidelity of JMC morphology is significantly affected by the loss of JPH2.

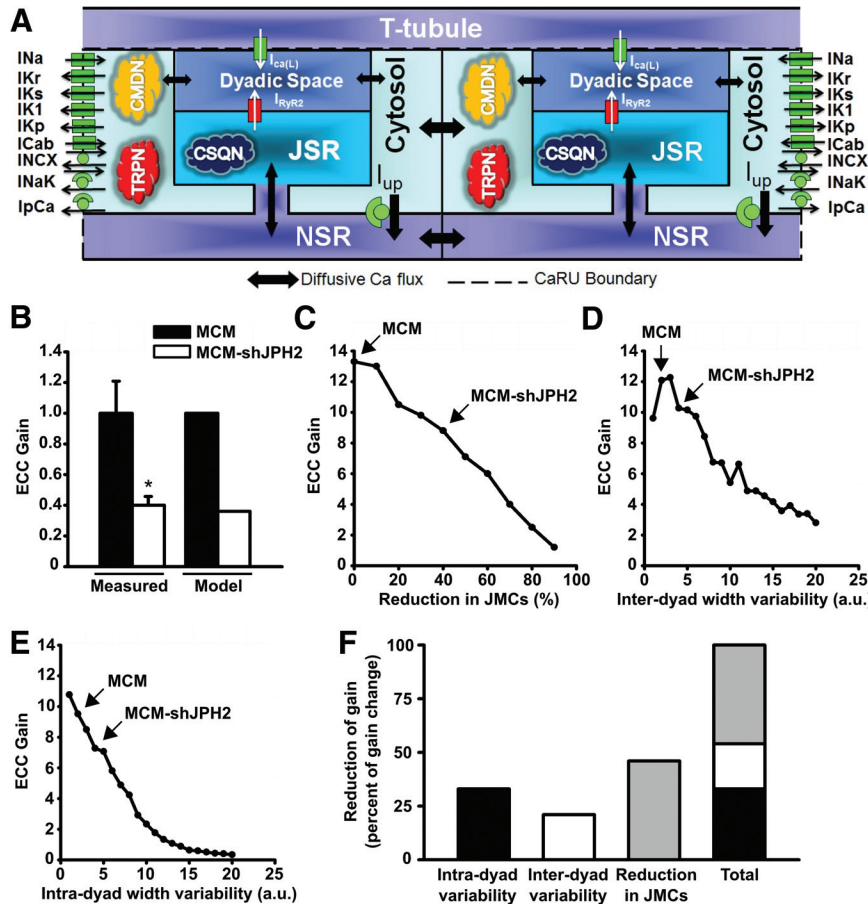


Figure 6. Computational analysis reveals effect of junctional membrane complexes (JMC) alterations on excitation-contraction (EC) coupling gain. A, Schematic representation of the novel computational model of discrete Ca^{2+} release in a cardiomyocyte. The different Ca^{2+} sources and sinks, as well as the various ion channels and Ca^{2+} binding proteins incorporated in the model, are shown. EC coupling gain is defined as the amount of Ca^{2+} released from the sarcoplasmic reticulum (SR) per unit of Ca^{2+} entering the cell from the extracellular space (T-tubule). B, Comparison of EC coupling (ECC) gain in myocytes from MCM and MCM-shJPH2 (α -MerCreMer-junctophilin-2 knock-down) mice, as measured with Ca^{2+} imaging (see Figure 2B) and predicted by the computational model. C through E, Simulations reveal the effect of a reduced number of JMC (C), an increase in interdyad width variability (D), and an increase in intradyad width variability (E) on EC coupling gain. Arrows indicate model outcomes for MCM and MCM-shJPH2 mice. F, Bar chart showing the individual and cumulative contributions of each parameter on EC coupling gain.

The T-tubular system permits the formation of larger numbers of JMCs within cardiomyocytes. T-tubule remodeling has been demonstrated in rats with pressure overload-induced heart failure²¹ and patients with congestive heart failure.²² In a recent study, heart failure development was correlated with progressive defects in T-tubule organization and a decline in JPH2 expression levels.²¹ Our findings provide, for the first time, a causal link between acute loss of JPH2 in MCM-shJPH2 mice and a reduction in the total number of JMCs and loss of T-tubules in ventricular myocytes. Normalization of the number of JMCs per sarcomere in MCM-shJPH2 mice intercrossed with JPH2 OE mice further underscores the specific role of JPH2 in maintaining JMC structure. Thus, our data demonstrate that JPH2 is an essential component of the JMC and that loss of JPH2 leads to disappearance of JMCs within affected cardiomyocytes.

Our studies in cardiomyocytes isolated from JPH2 knock-down mice revealed evidence for spontaneous Ca^{2+} releases from the SR (Figure 5). On the basis of findings in embryonic JPH2-deficient mice, it has been suggested previously that impaired coupling between VGCC and RyR2 might lead to impaired emptying of the SR, resulting in overload-induced diastolic SR Ca^{2+} release.⁴ However, our findings clearly revealed a reduction in overall SR Ca^{2+} content, which argues against this model (Figure 2H). Because cardiac RyR2 expression was unaltered after JPH2 knockdown, it is more likely that the loss of JPH2 impairs the ability of RyR2 to remain closed during diastole. The finding that JPH2 can be

coimmunoprecipitated with the use of anti-RyR2 antibody is also consistent with direct binding and regulation of RyR2 by JPH2. In fact, defective RyR2 regulation contributes to abnormal Ca^{2+} handling in failing hearts.²³ Thus, our data implicate JPH2 as a new allosteric regulator of RyR2 function and suggest that JPH2 downregulation can directly impair RyR2 Ca^{2+} release in failing hearts.

Moreover, we found that Ca^{2+} -dependent inactivation of VGCC was not altered in MCM-shJPH2 mice, which might be surprising given that the systolic SR Ca^{2+} transient was reduced (Figure 2). However, it is possible that diastolic SR Ca^{2+} leak due to increased RyR2 leak might elevate diastolic Ca^{2+} levels, thereby normalizing Ca^{2+} -dependent inactivation in MCM-shJPH2 mice. Therefore, it would be interesting to directly measure diastolic Ca^{2+} concentrations in future experiments. Finally, we found that Na^+ - Ca^{2+} exchange activity was reduced in myocytes from MCM-shJPH2 mice despite unaltered global expression levels. These results suggest that JPH2 might be required for proper subcellular targeting of Na^+ - Ca^{2+} exchange, but direct evidence for this is currently not available.

In conclusion, we have developed a novel approach to conditionally reduce JPH2 protein levels using RNA interference. Our studies uncovered the physiological roles of JPH2 in cardiac myocytes and implicate JPH2 as an important factor involved in the loss of cardiac contractility in heart failure, a key feature of this prevalent disease. In addition to determining the spacing between the plasmalemma and SR

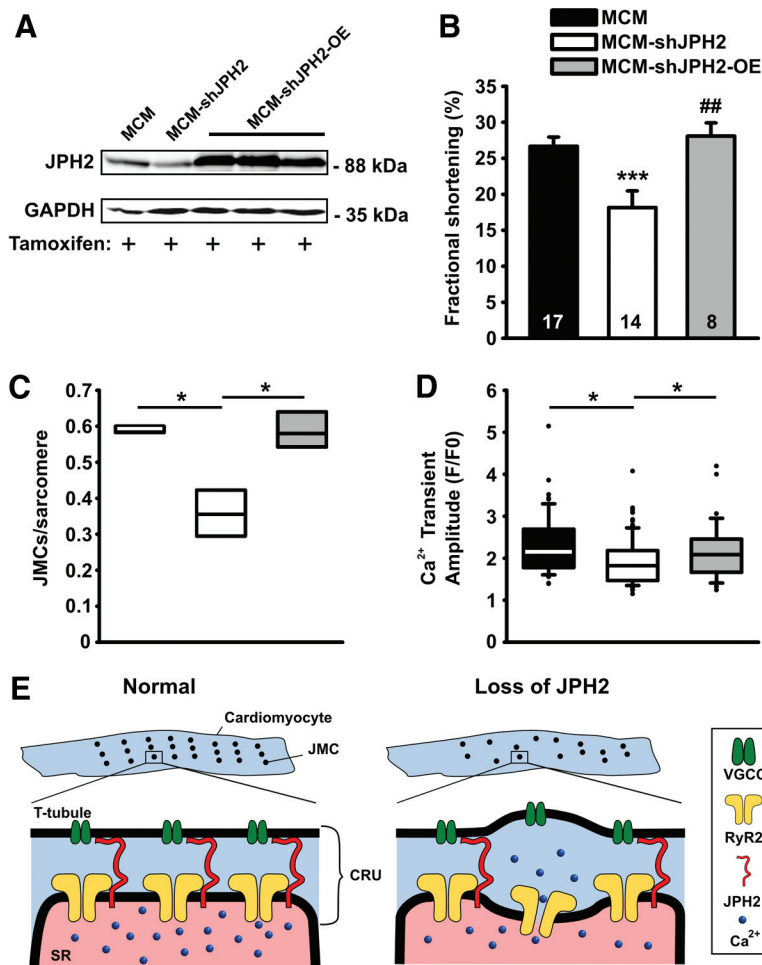


Figure 7. Junctophilin-2 (JPH2) knockdown effects can be rescued by transgenic overexpression of JPH2. A, Western blot demonstrating that crossing MCM-shJPH2 (α -MerCreMer–junctophilin-2 knock-down) mice with overexpressing (OE) mice restores JPH2 protein to supranormal levels in tamoxifen-treated mice. B, Fractional shortening measured with echocardiography. Data are represented as mean \pm SEM; number of mice is shown inside bars. C, Box plot indicating number of JMC per sarcomere, as measured by electron microscopy (n=400 sarcomeres per group). D, Box plot of Ca^{2+} transient amplitudes measured in isolated cardiomyocytes. E, Proposed model of the role JPH2 in cardiac myocytes. In normal ventricular myocytes (left), JMC are distributed evenly across sarcomeres. Each JMC contains calcium release units (CRU) comprised of voltage-gated Ca^{2+} channels (VGCC) on the sarcolemmal T-tubules and intracellular Ca^{2+} release channels/RyR2 (type 2 ryanodine receptors) on the sarcoplasmic reticulum (SR). Loss of JPH2 expression leads to reduced numbers of functional JMC per sarcomere, increased variability of the distance between the T-tubule and SR membranes, and defective RyR2 inactivation. * $P < 0.05$, *** $P < 0.001$ vs MCM control, # $P < 0.05$, ## $P < 0.01$ vs MCM-shJPH2.

membrane, JPH2 is also required for the structural integrity of JMCs in myocytes. Computational analysis provided further quantitative insights into the relative importance of each of these subcellular defects related to impaired EC coupling. Moreover, we found that JPH2 associates with and facilitates RyR2 inactivation, thereby preventing diastolic SR Ca^{2+} leak. This dual functional role for JPH2 in cardiomyocytes may have implications for the development of new therapeutic strategies for heart failure.

Acknowledgments

The authors thank Evelyn Brown and Margaret Gondo for technical assistance with electron microscopy, Dr Ivone Bruno for assistance with Northern blotting, Dr Tom Cooper for providing the α MHC plasmid, and Dr Chu-Xia Deng for providing pBS/U6-LoxP and pBS/U6-ploxPneo plasmids.

Sources of Funding

R.J.v.O. is the recipient of the 2008–2010 American Physiological Society Postdoctoral Fellowship in Physiological Genomics. N.G. is the recipient of a 2010–2012 American Heart Association Predoctoral Fellowship. Y.R. is the Fred Saigh Distinguished Professor at Washington University in St Louis, MO, and is supported by National Institutes of Health/National Heart, Lung, and Blood Institute grants R01-HL033343 and R01-HL049054 and National Science Foundation grant CBET-0929633. A.R.B. is supported by National Institutes of Health/National Eye Institute grants R01-EY017120 and P30-EY007551. M.J.A. is an Established Investigator of the American Heart Association and is supported by National

Institutes of Health grants R01-HD42569 and P01-HL94291 and the Mayo Clinic Windland Smith Rice Comprehensive Sudden Cardiac Death Program. X.H.T.W. is a W.M. Keck Foundation Distinguished Young Scholar in Medical Research and is supported by National Institutes of Health/National Heart, Lung, and Blood Institute grants R01-HL089598 and R01-HL091947, Muscular Dystrophy Association grant 69238, and the Fondation Leducq Award to the Alliance for Calmodulin Kinase Signaling in Heart Disease. Y.R., M.J.A., and X.H.T.W. are supported by a Fondation Leducq Award to the Alliance for Calmodulin Kinase Signaling in Heart Disease. Any opinions, findings, and conclusions or recommendations expressed in this material are those of the authors and do not necessarily reflect the views of the National Science Foundation.

Disclosures

None.

References

1. Bers DM. Cardiac excitation-contraction coupling. *Nature*. 2002;415:198–205.
2. Franzini-Armstrong C, Protasi F, Ramesh V. Shape, size, and distribution of Ca^{2+} release units and couplons in skeletal and cardiac muscles. *Biophys J*. 1999;77:1528–1539.
3. Song LS, Sobie EA, McCulle S, Lederer WJ, Balke CW, Cheng H. Orphaned ryanodine receptors in the failing heart. *Proc Natl Acad Sci U S A*. 2006;103:4305–4310.
4. Takeshima H, Komazaki S, Nishi M, Iino M, Kangawa K. Junctophilins: a novel family of junctional membrane complex proteins. *Mol Cell*. 2000;6:11–22.

5. Garbino A, van Oort RJ, Dixit SS, Landstrom AP, Ackerman MJ, Wehrens XH. Molecular evolution of the junctophilin gene family. *Physiol Genomics*. 2009;37:175–186.
6. Nishi M, Mizushima A, Nakagawara K, Takeshima H. Characterization of human junctophilin subtype genes. *Biochem Biophys Res Commun*. 2000;273:920–927.
7. Ito K, Komazaki S, Sasamoto K, Yoshida M, Nishi M, Kitamura K, Takeshima H. Deficiency of triad junction and contraction in mutant skeletal muscle lacking junctophilin type 1. *J Cell Biol*. 2001;154:1059–1067.
8. Landstrom AP, Weisleder N, Batalden KB, Bos JM, Tester DJ, Ommen SR, Wehrens XH, Claycomb WC, Ko JK, Hwang M, Pan Z, Ma J, Ackerman MJ. Mutations in JPH2-encoded junctophilin-2 associated with hypertrophic cardiomyopathy in humans. *J Mol Cell Cardiol*. 2007;42:1026–1035.
9. Matsushita Y, Furukawa T, Kasanuki H, Nishibatake M, Kurihara Y, Ikeda A, Kamatani N, Takeshima H, Matsuoka R. Mutation of junctophilin type 2 associated with hypertrophic cardiomyopathy. *J Hum Genet*. 2007;52:543–548.
10. Minamisawa S, Oshikawa J, Takeshima H, Hoshijima M, Wang Y, Chien KR, Ishikawa Y, Matsuoka R. Junctophilin type 2 is associated with caveolin-3 and is down-regulated in the hypertrophic and dilated cardiomyopathies. *Biochem Biophys Res Commun*. 2004;325:852–856.
11. Xu M, Zhou P, Xu SM, Liu Y, Feng X, Bai SH, Bai Y, Hao XM, Han Q, Zhang Y, Wang SQ. Intermolecular failure of L-type Ca²⁺ channel and ryanodine receptor signaling in hypertrophy. *PLoS Biol*. 2007;5:e21.
12. van Oort RJ, McCauley MD, Dixit SS, Pereira L, Yang Y, Respress JL, Wang Q, De Almeida AC, Skapura DG, Anderson ME, Bers DM, Wehrens XH. Ryanodine receptor phosphorylation by calcium/calmodulin-dependent protein kinase II promotes life-threatening ventricular arrhythmias in mice with heart failure. *Circulation*. 2010;122:2669–2679.
13. van Oort RJ, Respress JL, Li N, Reynolds C, De Almeida AC, Skapura DG, De Windt LJ, Wehrens XH. Accelerated development of pressure overload-induced cardiac hypertrophy and dysfunction in an RyR2–R176Q knockin mouse model. *Hypertension*. 2010;55:932–938.
14. Coumoul X, Shukla V, Li C, Wang RH, Deng CX. Conditional knockdown of fgfr2 in mice using Cre-Loxp induced RNA interference. *Nucleic Acids Res*. 2005;33:e102.
15. Sohal DS, Nghiem M, Crackower MA, Witt SA, Kimball TR, Tymitz KM, Penninger JM, Molkenkin JD. Temporally regulated and tissue-specific gene manipulations in the adult and embryonic heart using a tamoxifen-inducible Cre protein. *Circ Res*. 2001;89:20–25.
16. Cullen BR. Enhancing and confirming the specificity of MAI experiments. *Nat Methods*. 2006;3:677–681.
17. Faber GM, Rudy Y. Action potential and contractility changes in [Na(+)](i) overloaded cardiac myocytes: a simulation study. *Biophys J*. 2000;78:2392–2404.
18. Wehrens XH, Lehnart SE, Marks AR. Ryanodine receptor-targeted anti-arrhythmic therapy. *Ann N Y Acad Sci*. 2005;1047:366–375.
19. Chopra N, Yang T, Asghari P, Moore ED, Huke S, Akin B, Cattolica RA, Perez CF, Hlaing T, Knollmann-Ritschel BE, Jones LR, Pessah IN, Allen PD, Franzini-Armstrong C, Knollmann BC. Ablation of triadin causes loss of cardiac Ca²⁺ release units, impaired excitation-contraction coupling, and cardiac arrhythmias. *Proc Natl Acad Sci U S A*. 2009;106:7636–7641.
20. Gomez AM, Valdivia HH, Cheng H, Lederer MR, Santana LF, Cannell MB, McCune SA, Altschuld RA, Lederer WJ. Defective excitation-contraction coupling in experimental cardiac hypertrophy and heart failure. *Science*. 1997;276:800–806.
21. Wei S, Guo A, Chen B, Kutschke W, Xie YP, Zimmerman K, Weiss RM, Anderson ME, Cheng H, Song LS. T-tubule remodeling during transition from hypertrophy to heart failure. *Circ Res*. 2010;107:520–531.
22. Ohler A, Weisser-Thomas J, Piacentino V, Houser SR, Tomaselli GF, O'Rourke B. Two-photon laser scanning microscopy of the transverse-axial tubule system in ventricular cardiomyocytes from failing and non-failing human hearts. *Cardiol Res Pract*. 2009;2009:802373.
23. Wehrens XH, Lehnart SE, Reiken S, Vest JA, Wronska A, Marks AR. Ryanodine receptor/calcium release channel PKA phosphorylation: a critical mediator of heart failure progression. *Proc Natl Acad Sci U S A*. 2006;103:511–518.

CLINICAL PERSPECTIVE

Impaired cardiac muscle contraction is a hallmark of congestive heart failure. At the cellular level, excitation-contraction coupling requires proper communication of plasmalemmal voltage-gated Ca²⁺ channels and Ca²⁺ release channels on the sarcoplasmic reticulum within junctional membrane complexes (JMC). Disruption of the JMC structure is commonly seen in heart failure and is thought to contribute to contractile failure. Junctophilin-2 (JPH2) has recently been proposed to provide a structural connection between the plasma membrane and sarcoplasmic reticulum within the JMC, although its function has remained unclear because of the lack of adequate animal models. We have developed a novel approach to conditionally reduce JPH2 protein levels using RNA interference. Our studies revealed that acute knockdown of JPH2 leads to loss of cardiac contractility and heart failure in mice. JPH2 was found to determine the spacing between the plasmalemma and sarcoplasmic reticulum membrane, in addition to being required for the structural integrity of JMCs within myocytes. Computational analysis provided further quantitative insights into the relative importance of each of these subcellular defects related to impaired excitation-contraction coupling. Finally, our data showed that JPH2 associates with and facilitates type 2 ryanodine receptor inactivation, thereby preventing diastolic sarcoplasmic reticulum Ca²⁺ leak that could promote heart failure. Taken together, our studies suggest that downregulation of JPH2 could play an important role in the development of contractile dysfunction in heart failure.



SUPPLEMENTAL INFORMATION

Supplemental Methods

Recombinant Plasmids, and Transfection

Full-length mouse JPH2 cDNA was amplified from pCMS-RFP-JPH2¹ and subcloned into pcDNA3.1 (Invitrogen, Carlsbad, CA). For JPH2 RNAi transfections, 4 sets of short hairpin RNA (shRNA) oligonucleotides specific to mouse *JPH2* were cloned into pBS/U6-LoxP vector² (a kind gift from Dr. Chu-Xia Deng).

Generation of Transgenic Mice

JPH2 shRNA oligonucleotides (Forward: 5'-gcacttgaataacggcatattcaagagataggccgttattccaagtgcccttttg-3', Reverse: 5'-aattcaaaaaggcacttgaataacggcctatctcttgaatatgccgttattccaagtg-3') were ligated and cloned into pBS/U6-ploxPneo transgenic vector² (also a kind gift from Dr. Chu-Xia Deng) according to a previously described protocol³. Cardiac specific JPH2 overexpression (OE) mice were generated by subcloning mouse JPH2 cDNA into an α MHC transgenic vector (kindly provided by Dr. Thomas Cooper)⁴. The transgenic vectors were injected into the pronuclei of fertilized C57/BL6 oocytes, which were transferred to pseudopregnant recipients. Transgenic offspring (shJPH2) was crossed with MHC-MerCreMer (MCM) mice (Jackson laboratory, Bar Harbor, ME)⁵ to generate double transgenic mice (MCM-shJPH2). MCM-shJPH2 mice were crossed with OE mice to obtain triple transgenic MCM-shJPH2-OE mice. Three to five month old male MCM, MCM-shJPH2 and MCM-shJPH2-OE mice were treated with daily 100 μ l tamoxifen (Sigma-Aldrich Co., St. Louis, MO) intraperitoneal injections (~30 mg/kg) for 5 consecutive days. All mice were treated in accordance with Baylor College of Medicine Animal Care and Use Committee.

Northern Blot

Total RNA was extracted from left ventricular tissue using TRIzol reagent (Invitrogen, Carlsbad, CA). Ten μg of RNA was run in a 15% denaturing urea gel, and transferred to a Hybond N+ membrane (GE Healthcare, UK). A JPH2 probe was prepared using the *mirVana* probe preparation kit (Ambion, Austin, TX), following the kit procedures.

RT-PCR

One μg of RNA was reverse transcribed using Superscript II and oligo(dT) primer (Invitrogen, Carlsbad, CA). RTPCR was performed in duplicate in 96-well plates using SYBR Green and a Mastercycler ep realplex (Eppendorf, Hamburg, Germany), as described ^{6, 7}. Expression levels were compared using the relative Ct method.

Western Blotting

Heart lysates were prepared from flash-frozen mouse hearts as described previously ⁸. Heart lysate aliquots were size-fractionated on 6% (for RyR2), 7.5% (for JPH2), 12% (for Cav1.2, NCX1, SERCA2a, CaMKII, and GAPDH), or 15% (for PLN) SDS-polyacrylamide gels. Only for PLN-monomer blots, heart lysates were heated at 70°C for 10 min in 1x sample loading buffer containing 5% β -mercaptoethanol before loading on gels. The resolved gels were electro-transferred on PVDF membranes. The membranes were probed with anti-pSer2808-RyR2 (1:1,000; ⁸), anti-pSer2814-RyR2 (1:500; ⁸), anti-pSer16-PLN (1:5,000), or anti-pThr17-PLN (1:2,500) (both from Badrilla Ltd., Leeds, United Kingdom) phosphoepitope-specific antibody, and/or anti-Cav1.2 (1:200; Alomone Labs, Jerusalem), or anti-NCX1 (1:500; Swant, Bellinzona, Switzerland), or anti-SERCA2a (1:500; Santa Cruz Biotechnology, Santa Cruz, CA) polyclonal antibody, or an anti-JPH2 antibody raised against a synthetic peptide consisting of the amino acid

sequence 458-CRPRESQQLHERETPQPEG-475 and/or anti-RyR2 (1:5,000), or anti-PLN (1:1,000) (both Thermo Fisher Scientific (Pierce), Rockford, IL), or anti-GAPDH (1:5,000; Millipore, Temecula, CA) monoclonal antibody at 4°C overnight or at room temperature for 4 h. Blots were developed using Alexa-Fluor680-conjugated anti-mouse (Invitrogen Molecular Probes, Carlsbad, CA) and/or IR800Dye-conjugated anti-rabbit fluorescent secondary antibodies (Rockland Immunochemicals, Gilbertsville, PA), and scanned on an Odyssey infrared scanner (Li-Cor, Lincoln, NE). Integrated densities of protein bands were measured using ImageJ Data Acquisition Software (National Institute of Health, Bethesda, MD). Protein-signal densities were normalized to the corresponding GAPDH-signal densities, while phosphorylation signal densities were normalized to the corresponding total protein-signal densities, and used for plotting data.

Co-Immunoprecipitation Assay

In order to immunoprecipitate RyR2 from lysates, an anti-RyR2 antibody (Thermo Scientific, Rockland, IL) was incubated with Protein A-Sepharose beads (Rockland, Gilbertsville, PA) at RT for 1 h. Following which, this antibody attached beads were incubated with heart-lysate aliquots, containing 500 µg total protein, in a reaction volume of 300 µL at 4°C overnight. The reaction volume was made up with the homogenization buffer. At the end of the incubation, beads were washed with the homogenization buffer and then resuspended in 2x LDS buffer (Invitrogen, Carlsbad, CA) containing β-mercaptoethanol. The samples were heated at 50°C for 10 min, and were subjected to Western Blotting as described above.

Immunohistochemistry

Isolated cardiomyocytes were fixed in 2% paraformaldehyde for 10 min followed by 100 mM glycine in PBS (pH 7.4) for 10 min. Cells were washed twice for 10 min in PBS and permeabilized in PBS with 0.1% Triton X-100 for 10 min. Following two 10 min washes in PBS, the cells were incubated overnight at 4°C in antibody buffer (75 mM NaCl, 18 mM Na₃ citrate, 2% goat serum, 1%

BSA, 0.05% Triton X-100, 0.02% NaN₃, pH7.4) with mouse monoclonal RyR2 antibody (Thermo Scientific-Affinity BioReagents, Rockford, IL) and rabbit polyclonal Ca_v1.2 antibody (Alomone Labs, Jerusalem, Israel). The cells were washed twice for 10 min in wash buffer (75 mM NaCl, 18 mM Na₃ citrate, 0.05% Triton X-100, pH7.4) and incubated in antibody buffer with anti-mouse Alexa 568 and anti-rabbit Alexa 488 secondary antibodies (Invitrogen, Carlsbad, CA) for 2 hrs. Cells were resuspended in 50 µl mounting buffer (90% glycerol, 10% 10x PBS, 2.5% triethylenediamine, 0.02% NaN₃) and transferred to frosted slides. Isolated cardiomyocytes were resuspended in HEPES buffer at room temperature, then plated on laminin-coated dishes in 1mL of HEPES buffer and incubated at 37°C for 15 min. Cells were then washed with HEPES buffer and incubated for 1hr at RT. Imaging was performed using a laser scanning confocal microscope (LSM 510, Carl Zeiss, Thornwood, NY) with a 63X oil immersion objective. Pearson's correlation coefficient for colocalization was assessed using Zen 2008 software (Carl Zeiss, Thornwood, NY).

Histology

Hearts were fixed in 4% buffered formaldehyde, dehydrated with ethanol and histoclear, and embedded in paraffin. Tissues were sectioned longitudinally (5 µm), and stained with hematoxylin and eosin using standard protocols⁹. Cardiomyocyte cross-sectional areas were measured in sections stained with wheat germ agglutinin as described before⁶.

Transthoracic Echocardiography

Mice were anesthetized using 1-2.0% isoflurane in 95%. Cardiac function was assessed using M-mode echocardiograms acquired with a VisualSonics VeVo 770 Imaging System (VisualSonics, Toronto, Canada), as described¹⁰.

Cardiomyocyte Isolation and Ca²⁺ Imaging

Mouse ventricular myocytes were isolated as described⁶. Briefly, the heart was removed following isoflurane anesthesia and rinsed in 0 Ca²⁺ Tyrode solution (137 mM NaCl, 5.4 mM KCl, 1 mM MgCl₂, 5 mM HEPES, 10 mM glucose, 3 mM NaOH, pH 7.4). The heart was cannulated through the aorta and perfused on a Langendorf apparatus with 0 Ca²⁺ Tyrode (3 ~ 5 minutes, 37 °C), then 0 Ca²⁺ Tyrode containing 20 µg/ml (0.104 a.u./ml) Liberase TH Research Grade (Roche Applied Science) for 10 ~ 15 minutes at 37 °C. After digestion, the heart was perfused with 5 ml KB solution (90 mM KCl, 30 mM K₂HPO₄, 5 mM MgSO₄, 5 mM pyruvic acid, 5 mM β-hydroxybutyric acid, 5 mM creatine, 20 mM taurine, 10 mM glucose, 0.5 mM EGTA, 5 mM HEPES, pH 7.2) to wash out collagenase. The left ventricle of the heart was minced in KB solution and gently agitated, then filtered through 210 µm polyethylene mesh. After settling, ventricular myocytes were washed once with KB solution, and stored in KB solution at room temperature before use. Ventricular myocytes were incubated with 2 µM Fluo-4-acetoxymethyl ester (Fluo-4 AM, Invitrogen, Carlsbad, CA) in normal Tyrode solution containing 1.8 mM Ca²⁺ for 30 minutes at RT. Cells were then washed with dye-free normal Tyrode solution for 15 minutes for de-esterification and transferred to a chamber with a pair of parallel electrodes on a laser scanning confocal microscope (LSM 510, Carl Zeiss, Thornwood, NY) After being paced at 1 Hz for at least 2 minutes and steady state Ca²⁺ transients were observed, pacing was stopped for 45 seconds and spontaneous Ca²⁺ release events and Ca²⁺ sparks were counted. Steady state SR Ca²⁺ content was estimated by rapid application of 10 mM caffeine after pacing.

T-Tubule Imaging and Analysis.

T-Tubules of ventricular myocytes was visualized by Di-8-ANEPPS staining (10 µM for 10 min) in normal Tyrode solution with 1.8 mM Ca²⁺. Quantitative analysis of spatial integrity of T-Tubules was modified from previous studies^{11, 12} and was performed with ImageJ software (<http://rsb.info.nih.gov/ij/>). Region of interest was selected within a cell and outside of nucleus.

Power spectrum was computed using Fast Fourier Transform (FFT). Normalized power at spatial frequency of $\sim 0.55 \mu\text{m}^{-1}$ (peak power at $\sim 0.55 \mu\text{m}^{-1}$ normalized to average power at spatial frequency of 0.2 to $0.4 \mu\text{m}^{-1}$) was used as an index of the spatial integrity of T-Tubules (TT-Power).

Electrophysiology

Membrane currents were measured using whole cell patch clamp techniques with an Axopatch 200B amplifier, DigiData 1440a digitizer and pCLAMP v.10 software (Molecular Devices, Sunnyvale, CA). Ventricular myocytes were perfused with normal Tyrode solution with 1.8 mM Ca^{2+} . Pipette resistances were 1.5 - 3 $\text{m}\Omega$ prior to sealing. Electrode solution contained 110 mM CsCl, 20 mM tetraethylammonium chloride, 10 mM glucose, 10 mM HEPES, and 5 mM Mg-ATP (pH 7.2 adjusted with CsOH). Cells were voltage clamped at -80 mV in whole cell configuration. Prior to recording the holding potential was changed from -80 mV to -40 mV to inactivate Na^+ current (I_{Na}). I-V curves were generated using 500 ms depolarizing voltage steps from -40 to +40 mV in 10 mV increments. All currents were normalized to cell capacitances before comparison.

Excitation-Contraction Coupling Gain

To investigate EC coupling gain, confocal Ca^{2+} imaging and whole cell patch clamp techniques were employed simultaneously¹³. Ten pre-pulses at 0.2 Hz were applied to equalize SR Ca^{2+} and the testing pulse was delivered 30 seconds later. The EC coupling gain is expressed as the ratio of the amplitude of Ca^{2+} transient ($\Delta F/F_0$) and the amplitude of $I_{\text{Ca,L}}$ (pA/pF). Data was analyzed offline using Clampfit (Axon Instruments, CA) and Zen 2008 (Carl Zeiss, Thornwood, NY).

Electron Microscopy

Small sections of left ventricular apex were fixed in 0.1 M sodium cacodylate buffer (pH 7.2) containing 2.5% glutaraldehyde, post-fixed in 1% tannic acid and transferred to 1% osmium tetroxide. Specimens were dehydrated through an acetone series and embedded in resin. Thin plastic sections (80 to 100 nm) were cut, stained with uranyl acetate and lead citrate, and imaged on a Tecnai G² Spirit BioTWIN (FEI Company, Hillsboro, OR) electron microscope.

Co-immunoprecipitation

Anti-RyR2 antibody (Thermo Scientific, Rockland, IL) was incubated with Protein A-Sepharose beads (Rockland, Gilbertsville, PA) at RT for 1 h and incubated with heart lysates containing 500 µg total protein. Beads were washed and resuspended in 2x LDS buffer (Invitrogen, Carlsbad, CA) containing β-mercaptoethanol. The samples were heated at 50°C for 10 min, and were resolved on SDS-PAGE gels.

Computational Model

The modifications of the Luo-Rudy myocyte simulation model ¹⁴ will be described in detail elsewhere. The discrete Ca²⁺ release myocyte model was paced to a steady state at a basic cycle length (BCL) of 1000 ms. The myocyte was then held at a membrane potential of -88 mV for 100 ms before being clamped at 0 mV for a duration of 100 ms. The depth of the dyad is defined as the distance between the voltage-gated Ca²⁺ channels (VGCC) and type 2 ryanodine receptors (RyR2).

Statistical Analysis

Data are expressed as mean ± SEM. Statistical significance of differences between experimental groups was compared using Student's *t*-test, one-way ANOVA with pairwise multiple comparisons performed using the Student-Newman-Keuls method as appropriate. If results failed a normality

test, the Wilcoxon rank sum or Kruskal-Wallis tests were used, as appropriate. A value of $P < 0.05$ was considered statistically significant.

Supplemental References

1. Landstrom AP, Weisleder N, Batalden KB, Bos JM, Tester DJ, Ommen SR, Wehrens XH, Claycomb WC, Ko JK, Hwang M, Pan Z, Ma J, Ackerman MJ. Mutations in JPH2-encoded junctophilin-2 associated with hypertrophic cardiomyopathy in humans. *J Mol Cell Cardiol.* 2007;42:1026-1035.
2. Coumoul X, Li W, Wang RH, Deng C. Inducible suppression of fgfr2 and survivin in ES cells using a combination of the RNA interference (RNAi) and the Cre-loxp system. *Nucleic Acids Res.* 2004;32:e85.
3. Shukla V, Coumoul X, Deng CX. RNAi-based conditional gene knockdown in mice using a u6 promoter driven vector. *Int J Biol Sci.* 2007;3:91-99.
4. Ladd AN, Taffet G, Hartley C, Kearney DL, Cooper TA. Cardiac tissue-specific repression of celf activity disrupts alternative splicing and causes cardiomyopathy. *Mol Cell Biol.* 2005;25:6267-6278.
5. Sohal DS, Nghiem M, Crackower MA, Witt SA, Kimball TR, Tymitz KM, Penninger JM, Molkenstein JD. Temporally regulated and tissue-specific gene manipulations in the adult and embryonic heart using a tamoxifen-inducible cre protein. *Circ Res.* 2001;89:20-25.
6. van Oort RJ, McCauley MD, Dixit SS, Pereira L, Yang Y, Respress JL, Wang Q, De Almeida AC, Skapura DG, Anderson ME, Bers DM, Wehrens XH. Ryanodine receptor phosphorylation by calcium/calmodulin-dependent protein kinase II promotes life-threatening ventricular arrhythmias in mice with heart failure. *Circulation.* 2010;122: 2669-2679.
7. van Oort RJ, van Rooij E, Bourajjaj M, Schimmel J, Jansen MA, van der Nagel R, Doevendans PA, Schneider MD, van Echteld CJ, De Windt LJ. MEF2 activates a genetic program promoting chamber dilation and contractile dysfunction in calcineurin-induced heart failure. *Circulation.* 2006;114:298-308.

8. Chelu MG, Sarma S, Sood S, Wang S, van Oort RJ, Skapura DG, Li N, Santonastasi M, Muller FU, Schmitz W, Schotten U, Anderson ME, Valderrabano M, Dobrev D, Wehrens XH. Calmodulin kinase II-mediated sarcoplasmic reticulum Ca²⁺ leak promotes atrial fibrillation in mice. *J Clin Invest*. 2009;119:1940-1951.
9. van Oort RJ, Respress JL, Li N, Reynolds C, De Almeida AC, Skapura DG, De Windt LJ, Wehrens XH. Accelerated development of pressure overload-induced cardiac hypertrophy and dysfunction in an RyR2-R176Q knockin mouse model. *Hypertension*. 2010;55:932-938
10. el Azzouzi H, van Oort RJ, van der Nagel R, Sluiter W, Bergmann MW, De Windt LJ. Mef2 transcriptional activity maintains mitochondrial adaptation in cardiac pressure overload. *Eur J Heart Fail*. 2010;12:4-12
11. Song LS, Sobie EA, McCulle S, Lederer WJ, Balke CW, Cheng H. Orphaned ryanodine receptors in the failing heart. *Proc Natl Acad Sci U S A*. 2006;103:4305-4310
12. Wei S, Guo A, Chen B, Kutschke W, Xie YP, Zimmerman K, Weiss RM, Anderson ME, Cheng H, Song LS. T-tubule remodeling during transition from hypertrophy to heart failure. *Circ Res*. 2010;107:520-531
13. Ullrich ND, Fanchaouy M, Gusev K, Shirokova N, Niggli E. Hypersensitivity of excitation-contraction coupling in dystrophic cardiomyocytes. *Am J Physiol Heart Circ Physiol*. 2009;297:H1992-2003
14. Faber GM, Rudy Y. Action potential and contractility changes in [Na(+)](i) overloaded cardiac myocytes: A simulation study. *Biophys J*. 2000;78:2392-2404.

Supplemental Figure Legends.

Legend Supplemental Figure 1. Inducible cardiac-specific JPH2 knockdown mice causes mortality and acute heart failure

a. Schematic representation of vectors used to express JPH2 and different shRNAs targeting JPH2 in HEK cells. **b.** Western blot analysis of HEK cell lysates after co-transfection with JPH2 and 4 different shRNAs or empty vector (e.v.), respectively. Mouse heart lysate (H) was used as positive control for JPH2 detection. **c.** Quantitative PCR analysis of OAS1 and STAT1 mRNA levels in cardiac tissue from MCM (n=7) and MCM-shJPH2 (n=7) mice, indicating the absence of interferon response activation. **d.** Left ventricular posterior wall thickness in diastole (LVPWd) of MCM (17) and MCM-shJPH2 (14) mice at 1 week after completion of tamoxifen administration. **e.** Bar graph showing normalized cardiomyocyte area calculated from wheat germ agglutinin (WGA) stained sections. Numbers indicate number of cells (number of mice). **f.** Bar graph showing increased lung weight to tibia length in MCM-shJPH2 mice compared to MCM. Numbers in bar indicate number of mice. **g.** Quantitative PCR analysis of cardiac stress markers Acta1, ANF, BNP, β MHC, and RCAN1-4 in hearts from MCM and MCM-shJPH2 mice (n=7 each group). Data are represented as mean \pm SEM; * P<0.05 versus MCM control.

Legend Supplement Figure 2. Altered morphology of T-Tubules following knockdown of JPH2.

a-b. Bright field (**a**) and confocal fluorescence images (**b**) of representative di-8-ANEPPS-stained single ventricular myocytes isolated from tamoxifen-treated MCM (left) and MCM-shJPH2 (right) mice. **c.** Respective high resolution views and binary imaged (threshold at mean pixel intensity) of areas within the red rectangles in panel b. **e.** Corresponding Fast Fourier transformed images of T-

Tubule images shown in panel c. **f.** Representative power vs. spatial frequency along the x axis computed using Fourier analysis. **g.** Bar graph showing normalized power at spatial frequency of $\sim 0.55 \mu\text{m}^{-1}$ (as indicated by the arrow in panel e). Scale bar = 10 μm . *** $P < 0.001$ versus MCM control. n = 21 cells from 5 tamoxifen-treated MCM and 6 MCM-shJPH2 mice.

Legend Supplemental Figure 3. Inducible cardiac-specific JPH2 knockdown does not alter expression and phosphorylation levels of other calcium-handling proteins.

a. Representative Western blots of cardiac tissue lysates from MCM (n=6) and MCM-shJPH2 (n=6) mice showing expression levels of $\text{Na}^+/\text{Ca}^{2+}$ -exchanger (NCX1), sarcoplasmic reticulum Ca^{2+} ATPase 2 (SERCA2) and calsequestrin 2 (Casq2). **b.** Bar graphs summarizing quantitative analyses of the Western Blots shown in **a.** Protein expression levels were normalized first to corresponding GAPDH levels and then to average MCM value. **c, e.** Representative Western blot analyses of cardiac tissue lysates from MCM (n=6) and MCM-shJPH2 (n=6) mice showing expression and phosphorylation levels of ryanodine receptor 2 (RyR2; panel **c**) and phospholamban (PLN; panel **e**) at protein kinase A site (pS2808) and calcium calmodulin kinase II site (pS2814). **d, f.** Bar graphs summarizing quantitative analyses of the Western Blots shown in **c** and **e** respectively. RyR2 and PLN phosphorylation levels were normalized first to respective total protein expression levels and then to average MCM value. Data are represented as mean \pm SEM.

Legend Supplemental Figure 4. Inducible cardiac-specific JPH2 knockdown decreases expression level of JPH2 and its interaction with RyR2 to similar extents.

a. Representative Western blots of cardiac tissue lysates and immunoprecipitates (IP) from MCM (n=4) and MCM-shJPH2 (n=5) mice showing expression levels of ryanodine receptor 2 (RyR2) and junctophilin 2 (JPH2). RyR2 was immunoprecipitated using anti-RyR2 antibody from cardiac lysates (right). **b.** Bar graphs summarizing quantitative analyses of the Western Blots shown in **a.**

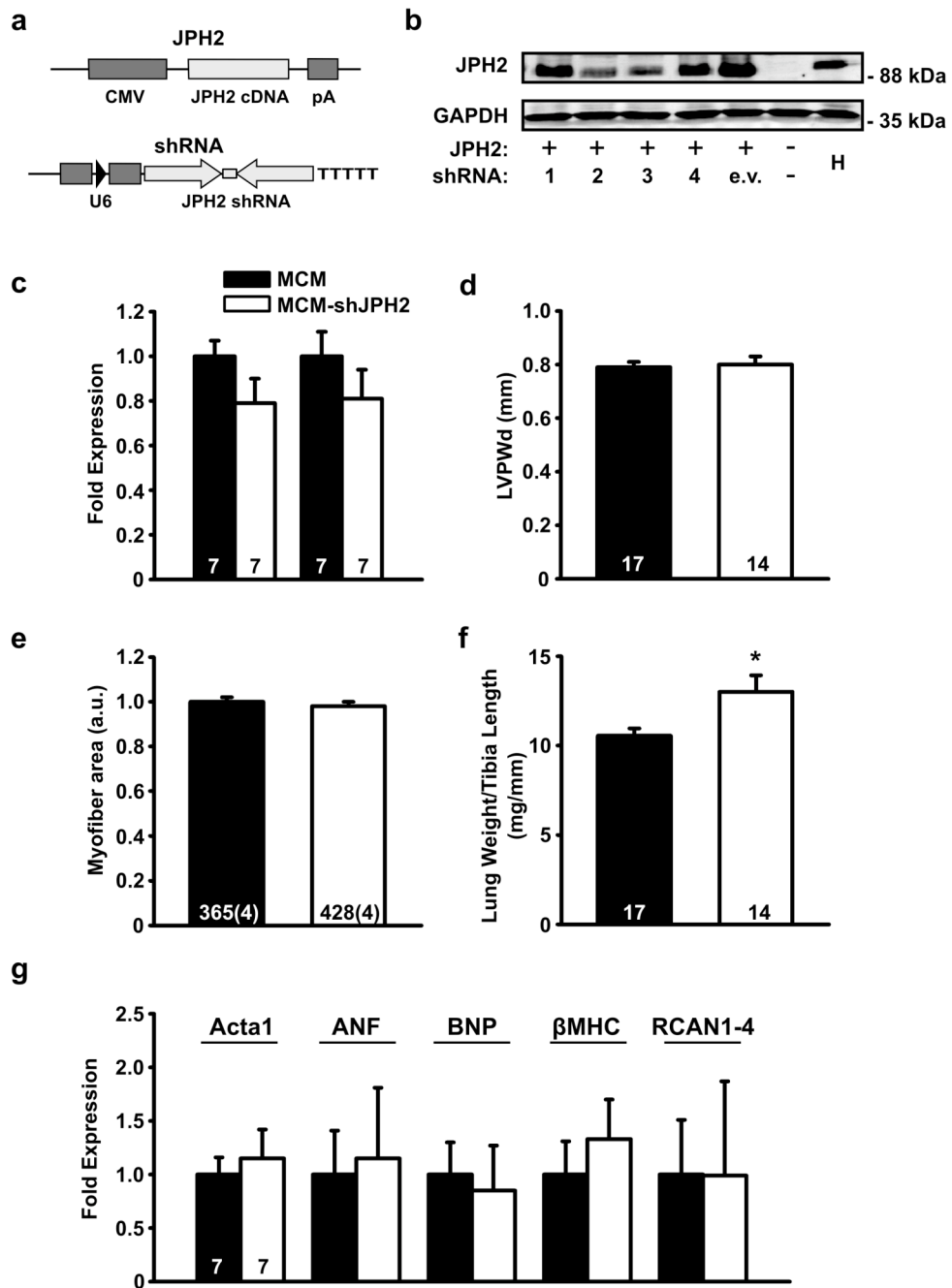
Protein expression levels were normalized to average MCM value. Data are represented as mean \pm SEM; * P<0.05 and **P<0.005, both versus MCM control.

Supplemental Table. Left ventricular echocardiographic parameters of MCM, MCM-shJPH2 line 21, MCM-shJPH2 line 38 and MCM-shJPH2 line38-OE mice at one week after finalizing tamoxifen treatment.

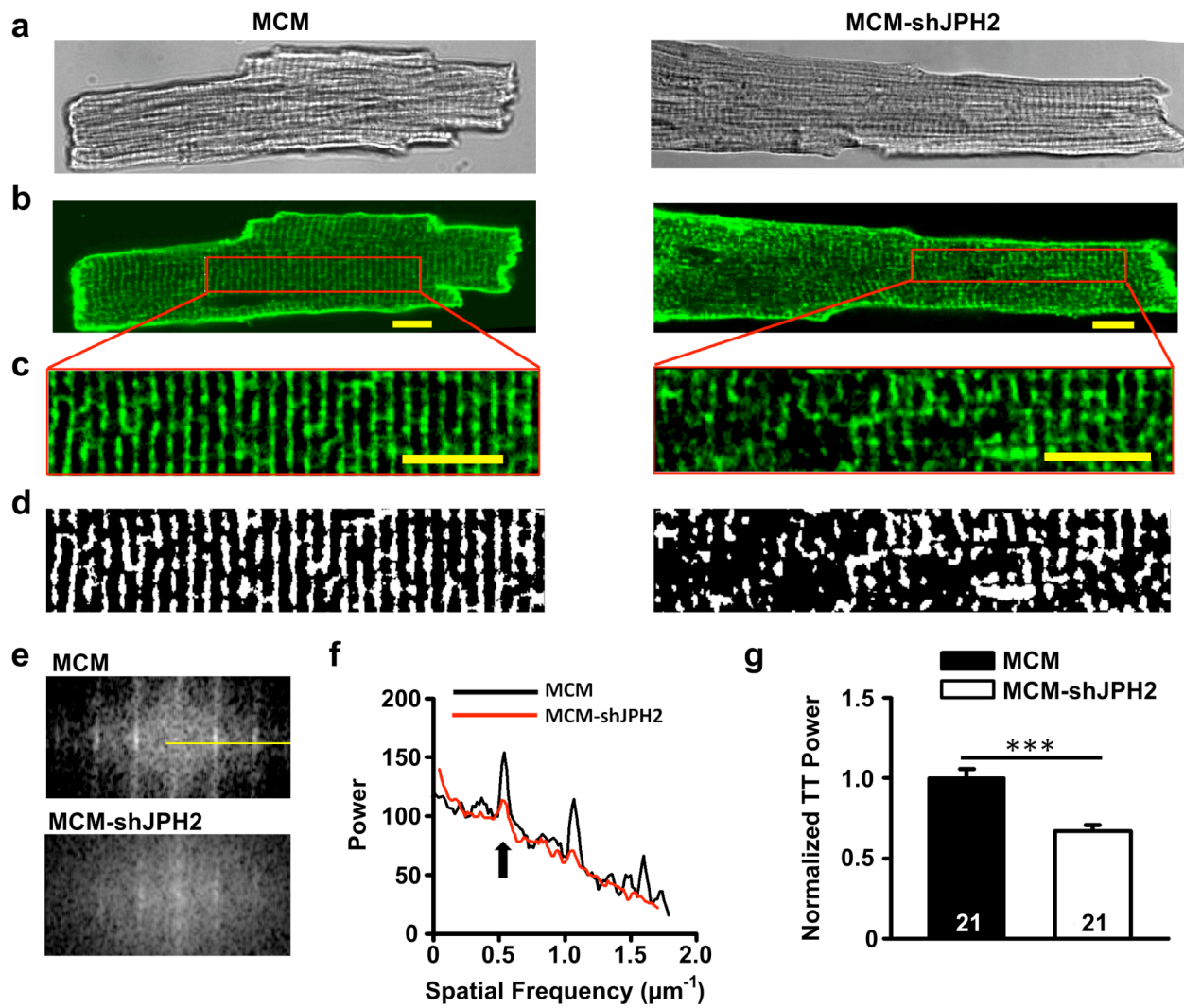
	MCM (n=17)	MCM-shJPH2 line 21 (n=11)	MCM-shJPH2 line 38 (n=14)	MCM-shJPH2-OE (n=8)
BW (g)	37.0 ± 0.8	35.2 ± 1.0	37.5 ± 1.7	35.0 ± 2.1
HR (b.p.m.)	450 ± 7 [#]	468 ± 10 ^{**,#}	485 ± 11 ^{*,###}	420 ± 4 ^{***}
ESD (mm)	3.19 ± 0.07	4.11 ± 0.13 ^{***,###}	3.89 ± 0.16 ^{***,##}	3.16 ± 0.20
EDD (mm)	4.35 ± 0.06	4.80 ± 0.07 ^{**,#}	4.73 ± 0.08 ^{**,#}	4.37 ± 0.18
EF (%)	52.0 ± 2.2	30.3 ± 3.7 ^{***,###}	36.7 ± 4.3 ^{**,#}	54.2 ± 3.0
FS (%)	26.7 ± 1.3	14.5 ± 1.9 ^{***,##}	18.2 ± 2.3 ^{**,#}	28.1 ± 1.8
IVSs (mm)	0.86 ± 0.01	0.76 ± 0.02 ^{***,#}	0.82 ± 0.02	0.83 ± 0.01
IVSd (mm)	0.76 ± 0.01	0.71 ± 0.02	0.76 ± 0.02	0.74 ± 0.01
LVPWs (mm)	1.13 ± 0.02	1.02 ± 0.06	1.03 ± 0.05	1.02 ± 0.03
LVPWd (mm)	0.79 ± 0.02	0.83 ± 0.04	0.80 ± 0.03	0.72 ± 0.03

BW = body weight; HR = heart rate; b.p.m. = beats per minutes; ESD = end-systolic diameter; EDD = end-diastolic diameter; EF = ejection fraction; FS = left ventricular fractional shortening; IVS = intraventricular septal wall thickness (s, systole d, diastole); LVPW = left ventricular posterior wall thickness (s, systole d, diastole). Data are expressed as mean ± SEM. * $P < 0.05$, ** $P < 0.01$, *** $P < 0.001$ versus MCM. # $P < 0.05$, ## $P < 0.01$, ### $P < 0.001$ versus MCM-shJPH2-OE.

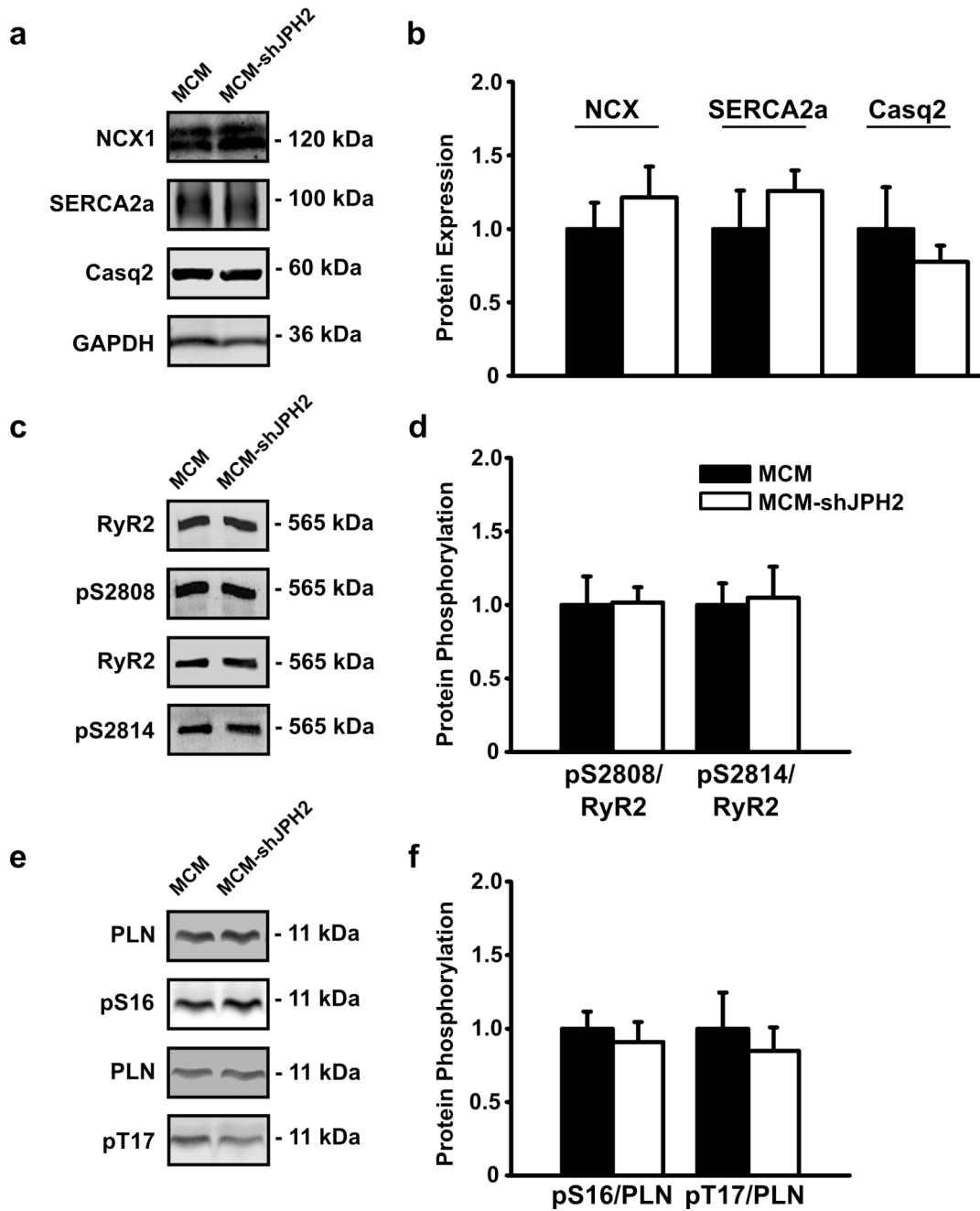
Supplemental Figure 1.



Supplemental Figure 2.



Supplemental Figure 3



Supplemental Figure 4.

